33RD CONGRESS
OF THE INTERNATIONAL COUNCIL
OF THE AERONAUTICAL SCIENCES
STOCKHOLM, SWEDEN, 4–9 SEPTEMBER, 2022

ICAS 2022 SWEDEN

ANALISIS OF LOW-SPEED AERODYNAMIC CHARATERISTICS OF BUSEMANN BIPLANE AIRFOIL INSTALLED HIGH LIFT DEVICES

ThaiDuong Nguyen[1], Masato Taguchi[1], Masashi Kashitani[1] & Kazuhiro Kusunose[2]
[1]Department of Aerospace Engineering, National Defense Academy of Japan, Japan.
[2]Formerly Japan Aerospace Exploration Agency, Japan

Abstract

In this paper, the effects of leading-edge and trailing-edge flaps on the low-speed performance of the Busemann supersonic biplanes are clarified by wind tunnel tests. The staggered models, which change the relative position of the upper and lower element in the axial direction, incorporated flaps are also investigated. The measuring system consists of the three-component balance system and a turntable placed in the test section's sidewall. The position of the hinges of flaps is 0.3*c* (where *c* is the chord length of the biplane element) away from the leading and trailing edges. The deflections of the leading-edge flap are 0° and 15°. The trailing-edge flaps varied from 0° to 45°. The stagger values, where the upper element is set forward to the lower element, are 0.25*c* and 0.5*c*. The results of single configurations (here, the upper and lower elements of the Busemann biplane are treated as single configurations) showed that the lift and drag increased when flaps were installed. The lift slopes are nearly constant even though the deflection of the trailing-edge flap increases. The leading-edge flap increases lift slope in both upper and lower elements. The biplane configurations show the increment in lift and drag when flaps are installed, similar to the conventional monoplane wing. The lift slope increases when the deflection of the trailing-edge flap increases. Also, the contribution of the lower element to total lift and total drag of the biplane decreases when flap deflection increases at angles of attack above 0°. The leading-edge flap and the stagger make the lift slope increase. Both flaps and stagger also increase the maximum lift, decreasing the stall angle compared with the baseline model. The contribution of the lower element to total lift and drag decreases at angles of attack above 0° when the stagger increases.

Keywords: Busemann Biplane, Low-speed Aerodynamic Characteristics, Flaps, Staggered models.

1. Introduction

The Busemann biplane concept is proposed to reduce the sonic boom in supersonic flight [1-2]. At the design Mach number, the shock waves are canceled between the upper and lower elements. In previous studies, the two-dimensional wing shows impressive performance at design Mach number compared with the diamond wing has the same thickness [1-2]. However, the problems of choked flow and flow hysteresis must be solved for the next steps of aircraft designs [3-5]. The choked flow's problem is that flow is accumulated between the biplane elements in the transonic and supersonic regimes. This phenomenon is similar to the choked flow generated by the inlet diffuser. On another hand, the problem of flow hysteresis is that the started Mach numbers, where the shock waves are canceled, are different when the flow velocity accelerates or decelerates. The phenomenon makes aircraft control unstable.

The biplane models incorporated with flaps and stagger are proposed to overcome the problems [6-9]. In previous numerical studies, the problems of choked flow and flow hysteresis are solved by using the simple leading and trailing edge flaps [6-7]. The staggered models are also considered [8-9]. However, the studies focused on transonic and supersonic regimes. For actual flight conditions, the low-speed aerodynamic characteristics are important for take-off and landing performances [10]. In previous studies, Kashitani et al. [11-12] investigated the flow field around the biplane wing with flaps by the smoke line visualizations. The lift coefficients are also estimated by the circulation theory of lift. The lift increment by using flaps are confirmed. However, the tests are conducted at small

angles of attack due to the unsteadiness of smoke lines. The balance results are required for the validation. Moreover, the staggered models also shows improvement when compared with the baseline model (the biplane model with no stagger). Previous studies investigated the stagger effects on the lows peed performances of the Busemann biplane [13-14]. The results shows the increments of lift slopes and drag coefficient. Therefore, the combination of stagger and flaps is expected to improve the wing's low-speed performances.

In this paper, the effects of leading-edge flaps and trailing-edge flaps on the two-dimensional low-speed performance of supersonic Busemann biplane are clarified by balance measurement. Also, the stagger wing incorporated flaps also investigated.

2. Experimental setup

2.1 Low-speed wind tunnel

Figures 1 (a) and (b) show the smoke wind tunnel utilized in the experiment. The wind tunnel is a suction type with a test section of 2000 mm length × 150 mm width × 1500 mm height. The maximum flow velocity is 26 m/s. The wind tunnel is equipped with a smoke generator (SC-3, Kanto Chemical Co., Ltd.), which enables visualization of the flow field around the test model.

2.2 The balance systems

In wind tunnel tests, a three-component force balance system (ML-3FM2, Izumi Sokki Co. Ltd.) are used to measure the aerodynamic forces. The measurable range of drag and lift of the balance is ±20 N. In the wind tunnel tests, the balance systems measure the aerodynamic forces acting on each element of the biplane separately. The systems consist of a balance and a turntable placed in the test section sidewall are used to adjust the angles of attack. The unmeasured wing element was fixed to the turntable. The gap between the model and the wind tunnel wall is 1.5 mm, which is determined from the displacement thickness of the boundary layer on the wind tunnel walls. The data was recorded by a data acquisition system (KEYENCE, NR-500). The system is advanced to clarify the low-speed performances of the baseline model and the staggered models in previous studies [13-14].

2.3 Experimental models

Figure 2 (a) - (c) shows an overview of the experimental models used in this study. The models were made of acrylic. The biplane element has a chord length *c* of 200 mm, a wing thickness *t* of 10 mm (*t*/*c* = 0.05), and a spacing between wing elements G of 100 mm (G/*c* = 0.5). The dimensions of the baseline configuration were calculated at a design Mach number of 1.7 [1-2].

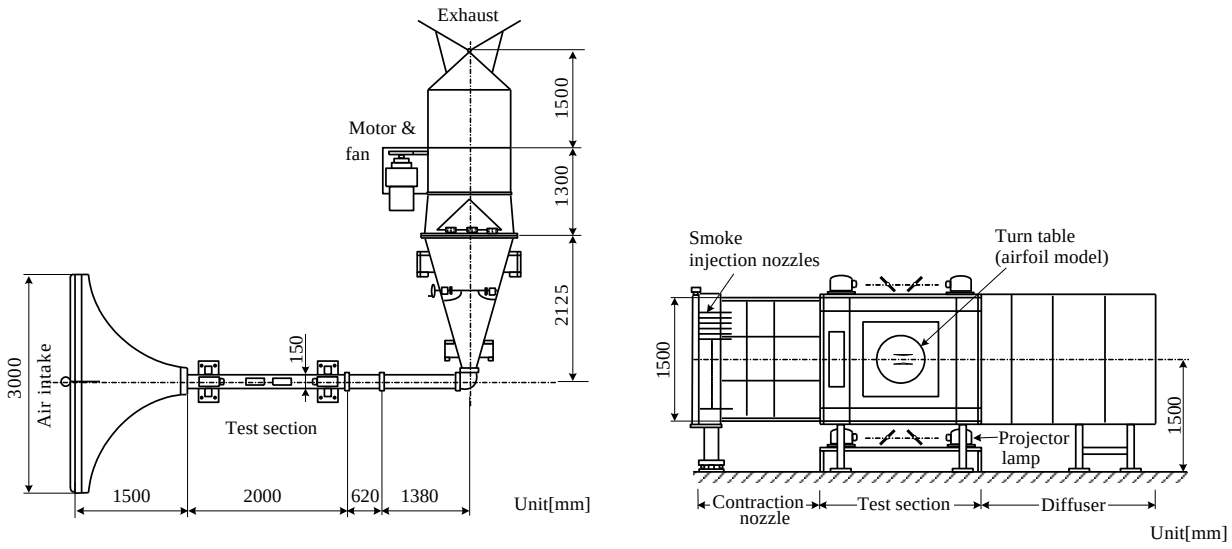

(a) Top view. (b) Side view.

Figure 1 Schematic diagram of the smoke wind tunnel.

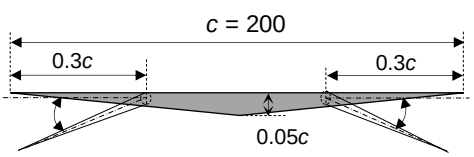

(a) Single upper element.

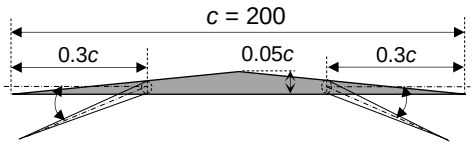

(b) Single lower element.

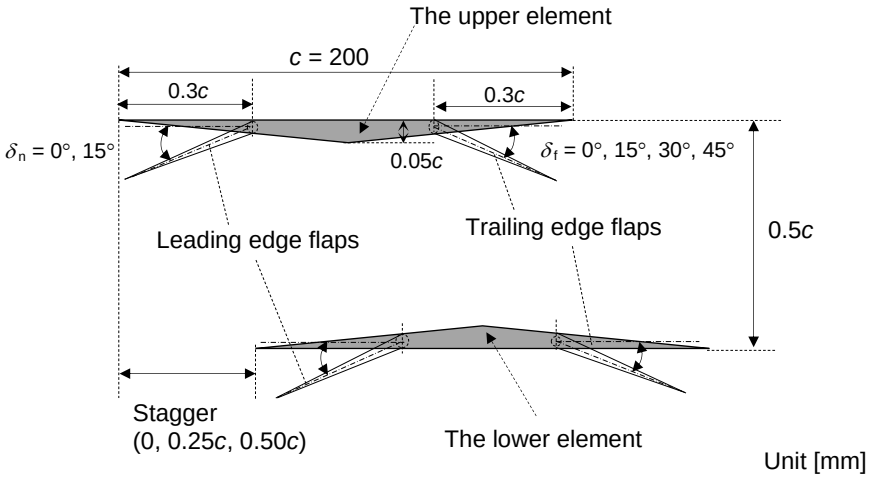

(c) The biplane model.

Figure 2 The experimental models.

The leading and trailing edge flaps were designed based on previous studies [7,11]. The position where the flaps are deflected is 0.3*c* from the leading edge or trailing edge, as the Fig. 2. The deflections of the leading-edge flap are δ_n = 0°, 15°, and the deflections of trailing-edge flaps are δ_f = 0°, 15°, 30°, 45°. Here, the leading-edge flap deployment is different with the cases in transonic regimes. In the tests of staggered models, the upper element was set forward for the staggered biplane, and stagger values are 0.25*c* and 0.5*c*. The detailed test cases will describe in experimental conditions.

2.4 Experimental conditions

Table 1 shows the experimental conditions. The flow velocity U_∞ is 15 m/s and Reynolds number *Re* is 2.1×10^5 based on the wing chord length. The angles of attack were varied from -30° to 30°.

In previous studies [13,14], the system was used to measure the aerodynamic forces of NACA0012 and the Busemann biplane airfoil (Baseline configuration). The results have good agreement with numerical simulations and reference data, shown that this measurement setup can acquire two-dimensional aerodynamic characteristics of single configurations and biplane configuration.

The tests of a single configuration are separately conducted with upper and lower elements. When the deflection of the leading-edge flap δ_n is 0°, the deflection of trailing-edge flaps δ_f are varied 0° to 45°. When the leading-edge flap δ_n is 15°, the trailing edge flap δ_f is 30°.

In the tests of biplane configurations, when the leading-edge flap δ_n is 0°, the trailing edge flaps δ_f are varied 0° to 45°. At these times, the stagger value *St* is 0 (No stagger). The tests aim to clarify the effects of the trailing-edge flap on the aerodynamic characteristics of the Busemann biplane. Next, in the case of δ_n = 0° and δ_f = 30°, the stagger value *St* is set to 0, 0.25*c* and 0.5*c*, respectively. The tests aim to investigate the stagger effects on aerodynamic performances of Busemann biplane with trailing-edge flaps. Finally, in the case of δ_n = 15° and δ_f = 30°, the stagger value *St* is set 0 and 0.5*c*, respectively. The tests aim to investigate the effects of the combination of a leading-edge flap, trailing-edge flap, and stagger.

Table 1. Experimental conditions.

Parameters		
Flow velocity	15 m/s	
Reynold number	2.1×10^5	
The angle of attack	-30° ~ 30°	
Balance measurement time	20 s	
Sampling frequency	5 Hz	
Single configuration	δ_n = 0°; δ_f = 0°, 15°, 30°, 45°	Upper element
		Lower element
	δ_n = 15°; δ_f = 30°	Upper element
		Lower element
Biplane configuration	δ_n = 0°; δ_f = 0°, 15°, 30°, 45°	Stagger *St* = 0
	δ_n = 0°; δ_f = 30°	Stagger *St* = 0, 0.25*c*, 0.5*c*
	δ_n = 15°; δ_f = 30°	Stagger *St* = 0, 0.5*c*

The total aerodynamic coefficients of the biplane model are defined by the sum of the elements in biplane configuration, as flowing equations.

$$C_{D\ total} = C_{D\ upper\ \_biplane} + C_{D\ lower\ \_biplane} \quad (1)$$

$$C_{L\ total} = C_{L\ upper\ \_biplane} + C_{L\ lower\ \_biplane} \quad (2)$$

Where the $C_{D\ total}$ and $C_{L\ total}$ are the total drag coefficient and total lift coefficient of the biplane model. In biplane configuration, $C_{D\ upper\ \_biplane}$, $C_{D\ lower\ \_biplane}$, $C_{L\ upper\ \_biplane}$, $C_{L\ lower\ \_biplane}$ are the drag coefficient of the upper element, the drag coefficient of the lower element, the lift coefficient of the upper element, the lift coefficient of the lower element, respectively.

3. Results and discussions

3.1 Results of single configuration

Figures 3, Figure 4, and Table 2 show the results of upper and lower wing elements which are treat as single configurations. The results are compared with baseline model in the previous study [13-14]. By comparing the results of single configurations with and without flap deflection, the flap effects on the single upper and lower elements are investigated.

Figure 3 shows the aerodynamic characteristics of a single upper element with flaps. In Fig. 3(a), when a trailing flap is installed, the lift increment is confirmed. When the deflection of the trailing-edge flap δ_f increases, the stall angle decreases. The stall angles are with 11°, 9°, 8°, 8°, and the maximum lift coefficients are 0.68, 1.14, 1.36, 1.49 in order of δ_f = 0°, 15°, 30°, 45°, respectively. The lift slopes are 0.88, 0.087, 0.093, 0.093. When δ_n = 15° and δ_f = 30°, the stall angle is 10°, and the maximum lift is improved to 1.63. The lift slope is 0.102. Compared with results of the trailing-edge flap model (δ_n = 0°, δ_f = 30°), the leading-edge flap shows the lift increase for angle larger than 7° and make the decrease of lift results at the angle smaller than -5°. In Fig. 3(b), when the trailing-edge flaps are installed, the drag increment is confirmed. The angle of attack, where minimum drag appears, decreases when the flap deflection increases, with -1°, -6°, -8°, and -10° in order of δ_f = 0°, 15°, 30°, 45°, respectively. Even the trailing-edge flaps are installed, the bucket shape distribution of drag coefficient is reserved. When δ_n = 15° and δ_f = 30°, the leading flap shows the drag increment for angle smaller than 0° and make the decrease of lift results at the angle of 0° to 11° compared with results of the trailing-edge flap model (δ_n = 0°, δ_f = 30°). For the angles larger than 11°, the leading-edge flap shows small increment in the drag coefficient. Figure 3(c) shows the lift to drag ratio of a single upper element with flaps.

Figure 4 shows the aerodynamic characteristics of a single lower element with flaps. In Fig. 4(a), when the trailing flap is installed, the lift increments are confirmed. When the deflection of trailing flap δ_f increases, the angle of attack where stall occurs decreases. The stall angles are 12°, 12°, 11°, 9°, and the maximum lift coefficient are 1.08, 1.45, 1.58, 1.62 in order of δ_f = 0°, 15°, 30°, 45°, respectively. The lift slopes are 0.88, 0.085, 0.084, 0.085, respectively. When δ_n = 15° and δ_f = 30°, the stall angle is 13°, and the maximum lift is improved to 1.75. The lift slope is 0.096. Compared with results of the trailing-edge flap model (δ_n = 0°, δ_f = 30°), the leading flap shows the lift improvement for angles larger than 10°, making the lift decrease at the angle smaller than 10°. In Fig. 4(b), when the trailing-edge flaps are installed, the drag increment is confirmed. The angle of attack, where minimum drag appears, decreases when the deflection of trailing flap δ_f increases. There are -2°, -5°, -7°, and -9° in order of δ_f = 0°, 15°, 30°, 45°, respectively. Even the trailing-edge flaps are installed, the bucket shape distribution of drag coefficient is reserved. When δ_n = 15° and δ_f = 30°, the leading flap shows the drag increments at angles smaller than -3° and make the decrease of drag results at the angle larger than -3°. Also, the leading-edge flap impressively decreases drag from 0° to 13°. So, the leading-edge flap increases the lift and decreases the drag for the lower element at angles larger than 10°. Figure 4(c) shows the lift to drag ratio of a single lower element with flaps.

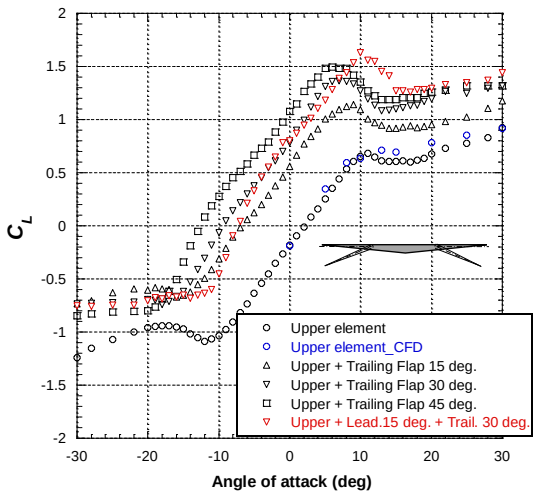

(a) Lift coefficient.

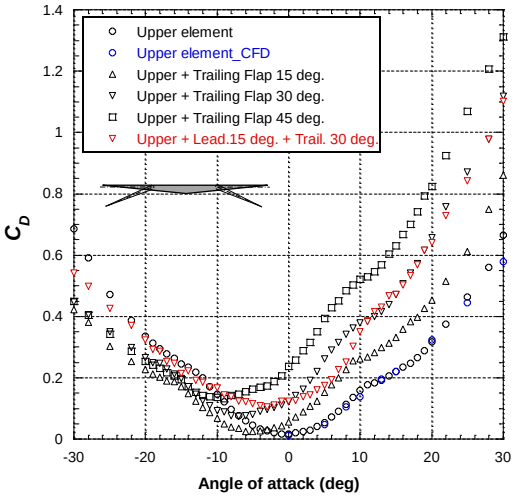

(b) Drag coefficient.

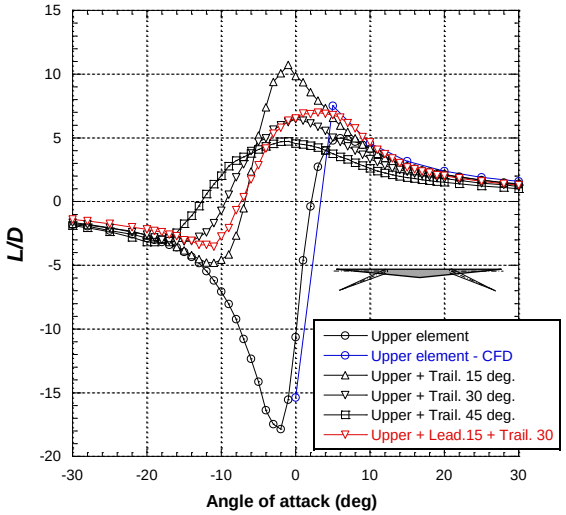

(c) Lift to drag ratio.

Figure 3 The aerodynamic characteristics of single upper element.

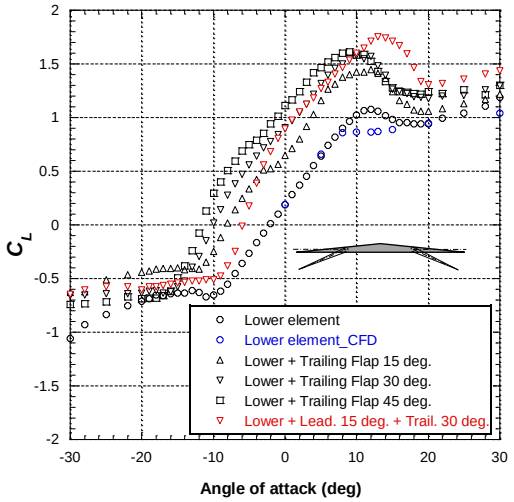

(a) Lift coefficient.

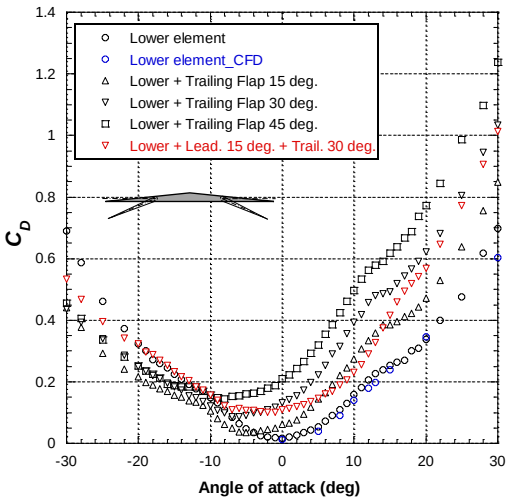

(b) Drag coefficient.

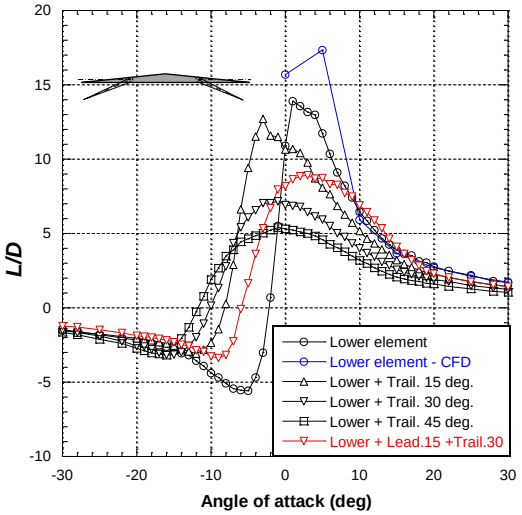

(c) Lift to drag ratio.

Figure 4 The aerodynamic characteristics of single lower element.

Table 2. Lift slopes of single configurations.

Single configurations	δ_n = 0° δ_f = 0°		δ_n = 0° δ_f = 15°	δ_n = 0° δ_f = 30°	δ_n = 0° δ_f = 45°	δ_n = 15° δ_f = 30°
	Exp.	**CFD**				
Upper element	0.088	0.088	0.087	0.093	0.093	0.102
Lower element	0.088	0.084	0.085	0.084	0.085	0.096

The results of single configurations show the increment of lift and drag when flaps are installed. The lift slope is nearly constant in the case of the upper element with the deflection of the trailing flap lower than 30°. In cases of the lower element, the lift slope decreases when the flap deflection increases. The leading-edge flap makes the lift slope increase in both upper and lower elements. The numerical results show good agreement with balance measurements.

3.2 Results of biplane configurations

3.2.1 Effects of trailing-edge flaps

Figure 5 and Table 3 show the aerodynamic characteristics of the biplane configuration with trailing-edge flaps. In this system, the aerodynamic characteristics of upper and lower element in biplane configuration are separately measured. The biplane's aerodynamic characteristics are the sum of those aerodynamic characteristics of the upper and lower elements. The results of the baseline model (the biplane model without flap deflections) are compared with CFD and previous studies.

In Fig. 5(a), when the trailing-edge flaps are installed, the lift increment is confirmed, and the stall occurs. When the deflection of the trailing-edge flap δ_f increases, the stall angle decreases. The stall angles are 9°, 7°, and 3°, and the maximum lift coefficient is 1.96, 2.16, and 2.26 when δ_f = 15°, 30°, and 45°, respectively. For the angle larger than 17°, the lift in all configurations is nearly constant. The lift slope increases when the deflection of the trailing-edge flap increases. The lift slopes are 0.129, 0.133, 0.137, 0.15 regarding to δ_f = 0°, 15°, 30°, 45°, respectively. In Fig. 5(b), when the trailing-edge flaps are installed, the angle of attack, where minimum drag appears, decrease when the flap deflection δ_f increase. The minimum drag are 0.084, 0.192, and 0.316 at -7°, -8°, and -13° in order of δ_f = 15°, 30°, 45°, respectively. When the angle of attack increases, the drag increment because of the trailing flap also increases. In Busemann biplane wing, the trailing-edge flap shows the similar trend as the conventional monoplane wing. Figure 5(c) shows the lift to drag ratio results.

Figures 6(a) and (b) show the ratio of the lower element to the biplane performance. Figure 6(a) shows the lift ratio of the lower wing to the total (biplane) lift. About 95% of the total lift is generated from the lower wing at the angle of attack larger than 20°. This result has the same tendency as the previous study of the tandem wing [17]. When the trailing-edge flaps are installed, the lift proportion of the lower wing decreases when the flap deflection δ_f increases at the angle of attack larger than 0°. At 20°, the lift proportions are about 83%, 73%, 57% when δ_f = 15°, 30°, 45°, respectively. The angle of attack, where the lift ratio suddenly changes, decreases as the flap deflection increases. The lift ratio increases when the flap deflection increases at angles of attack smaller than -13°. Figure 6(b) shows the drag ratio of t lower wing to the total (biplane) drag of biplane configuration. When the trailing-edge flaps are installed, the amount of change of drag ratio from the lower element in the range of ±30° is decreases. When δ_f = 45°, the drag ratio changes from 0.42 to 0.61 in the range of ±30°.

3.2.2 Effects of the combination of flaps and stagger

Figure 7 and Table 3 show the results of biplane configuration with a combination of flaps and stagger. In the tests, the trailing-edge flap δ_f = 30°, the leading-edge flap δ_n = 0°, 15°, and the stagger values *St* = 0, 0.25*c*, 0.5*c* are considered.

Figure 7 shows the aerodynamic coefficient results. In Fig. 7(a), the leading-edge flap (δ_n = 15°, δ_f = 30°) shows the lift increments from the angle of attack larger than 6° compared with the configuration of only 30° trailing-edge flap configuration (δ_n = 0°, δ_f = 30°). The stall angle increases from 7° to 10°, and the maximum lift coefficient increases from 2.15 to 2.4, respectively. At angles smaller than 6°, the leading flap makes the lift decrease. Next, the stagger effects are clarified. With the configuration of δ_n = 0° and δ_f = 30°, the lift coefficient has no significant difference at angles smaller than -5°. From -5° to 2°, the 0.25*c* stagger configuration shows a more significant lift than the 0.5*c* stagger configuration. The larger lift coefficient is generated with a larger stagger value at angles larger than 2°. The stall angle is 4°, and the maximum lift is about 2.14 in the 0.25*c* stagger configuration. In the case of 0.5*c* stagger configuration, the stall angle is 6°, and the maximum lift is 2.3. The stagger decreases the stall angle and increases the maximum lift compared with the configuration having no stagger. When the leading-edge flap is deflected (δ_n = 15°, δ_f = 30°), the 0.5*c* stagger configuration shows the stall at 8°, and the maximum lift is about 2.47. The stagger effects show a similar trend as the configuration with only trailing-edge flap (δ_n = 0°, δ_f = 30°). In Fig. 7(b), the leading-edge flap (δ_n = 15°, δ_f = 30°) decreases drag coefficient at angles larger than -4° and increases the drag coefficient at angles smaller than -4°. When the angle of attack increases, the drag decrement by leading-edge flap is nearly constant. Next, the stagger shows the drag increment at angles larger than 0° in trailing-edge flap configuration (δ_n = 0°, δ_f = 30°). The stagger shows no significant difference at the range of -2° to 5°. When the angle of attack increases, the drag increment because of the stagger also increases. The stagger effects show a similar trend as the configuration with leading-edge flap (δ_n = 15°, δ_f = 30°). Figure 7(c) shows the lift to drag ratio results.

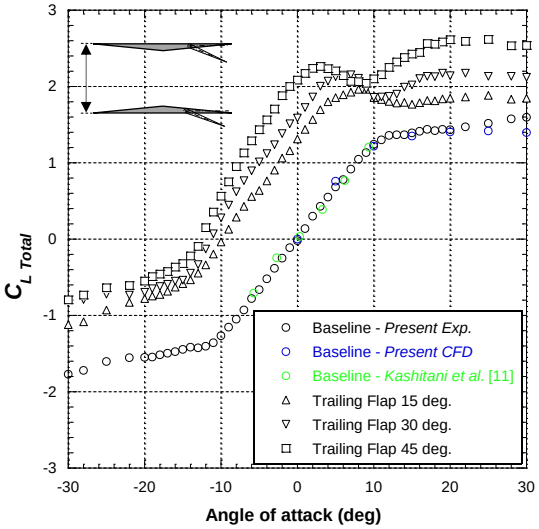

(a) Lift coefficient.

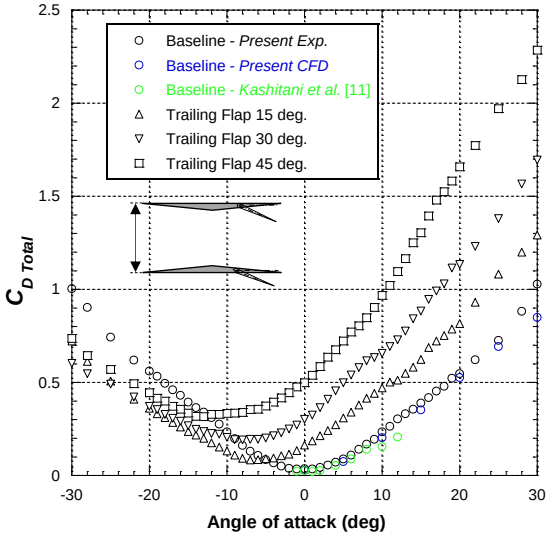

(b) Drag coefficient.

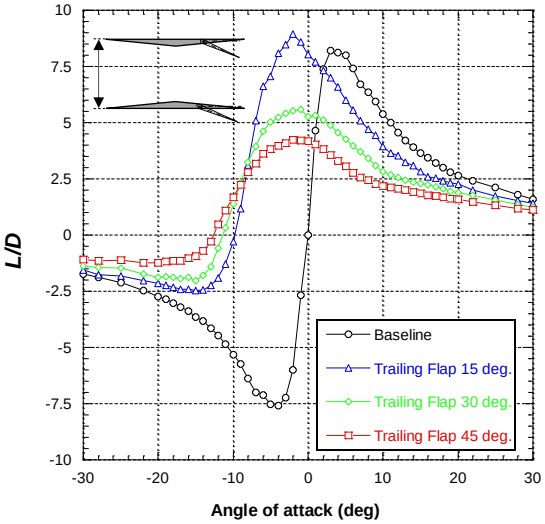

(c) Lift to drag ratio.

Figure 5 The aerodynamic characteristics of Busemann biplane installed trailing-edge flaps.

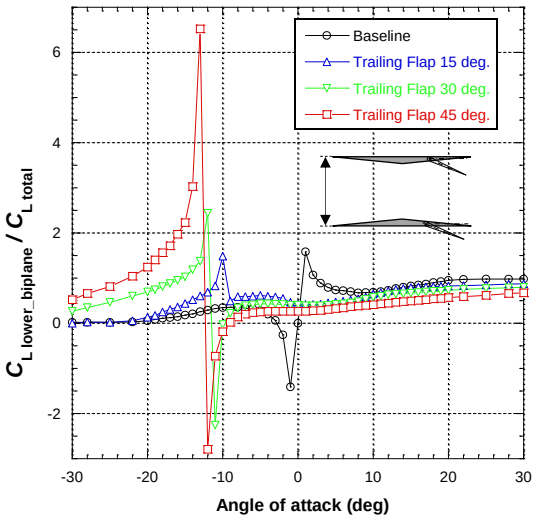

(a) Ratio for lift coefficient.

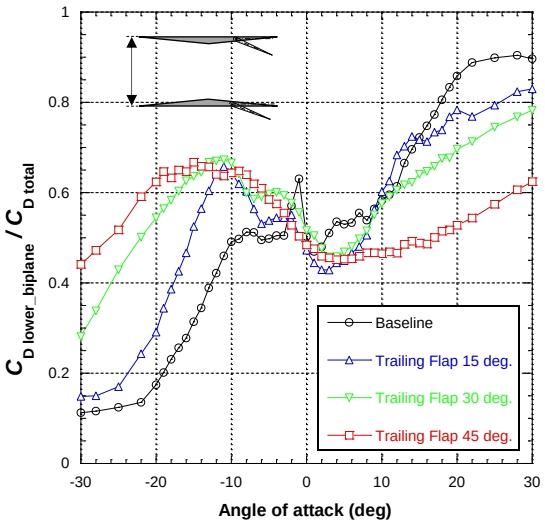

(b) Ratio for drag coefficient.

Figure 6 Ratios of the lower element to the biplane performances with trailing-edge flaps.

Figure 8(a) and (b) show the lift and drag ratio of the lower element distributed to the total results of the biplane configuration. In Fig. 8(a), the leading-edge flap (δ_n = 15°, δ_f = 30°) makes the lift ratio decrease at angles larger than -5° compared with the configuration having only trailing-edge flap (δ_n = 0°, δ_f = 30°). The lift ratio is nearly constant at the angles larger than 20°, with 0.73 for the configuration (δ_n = 0°, δ_f = 30°) and 0.65 for the configuration (δ_n = 15°, δ_f = 30°). The angle of attack, where the lift ratio suddenly changes, also increases from 11° to 8° when deflecting the leading-edge flap. The reason is the angle of attack where the total lift of biplane configuration approaches zero, as shown in Fig. 7(a). The stagger effects are shown in Fig. 8(a). In the case of δ_n = 0° and δ_f = 30°, the lift ratio decreases when the stagger value increases at angles larger than -11°. The lift ratio is almost constant at angles larger than 20°, with about 0.53 for the 0.25*c* stagger configuration and 0.47 for the 0.5*c* stagger configuration. The angle of attack, where the lift ratio suddenly changes, is -11° in 0.25c and 0.5*c* stagger configuration, the same as the model having no stagger. When the leading flap is deflected (δ_n = 15°, δ_f = 30°), the stagger makes the lift ratio decreases at angles larger than -7° compared with no stagger model, the same as the configuration with only trailing-edge flap (δ_n = 0°, δ_f = 30°).

Figure 8(b) shows the drag ratio of the lower wing distribute to the total results of biplane configuration. The leading-edge flap (δ_n = 15°, δ_f = 30°) makes the drag ratio of the lower element decrease at angles larger than 9° compared with the configuration with only trailing-edge flap (δ_n = 0°, δ_f = 30°). At the range of 9° to 30°, the curve of drag ratio when the leading-edge flap is deflected is nearly parallel with the results of no leading flap. The lower element distributed about 80% of total drag near -10° in the configuration with δ_n = 0° and δ_f = 30°. When the leading flap is deflected (δ_n = 15°, δ_f = 30°), the drag ratio is about 60%. In the cases of staggered models (δ_n = 0°, δ_f = 30°), the stagger makes the drag ratio of the lower wing decrease at the angle of attack larger than 0°. In the case of the 0.5*c* stagger model, the drag ratio is almost constant nearly 50% at angles larger than 20°. It means that the lower and upper element has nearly the same distribution to total drag. When the leading-edge flap is deflected (δ_n = 15°, δ_f = 30°), the stagger makes the drag ratio of the lower wing decrease at angles larger than 0° compared with the no stagger model, the same as the configuration with only trailing-edge flap (δ_n = 0°, δ_f = 30°).

Figure 9 shows the flow field around the biplane configuration with only trailing-edge flap (δ_n = 0°, δ_f = 30°). The stagger value are 0 and 0.5*c*, and the angles of attack are 0° and 10°, respectively. The flow direction is from right to left, as red arrows in the figure. The smoke lines between the airfoil elements can be visualized. In Fig. 9 (a), the flow on the upper surface of the upper element separated even at the angle of attack of 0°, as results in previous studies [11,12]. On the other hand, the smoke lines flow smoothly on the upper surface of the lower element from the leading edge to the position that trailing edge flap deflected. At 10°, the flow near the upper surface of the upper is largely separated. The flow on the upper surface of the lower element slightly separated at the leading edge. However, the smoke lines are pushed to the upper surface of the lower element when moving to downstream because the existence of the upper element. In Fig. 9(b), the flow separation on the upper surface of the upper element at 0° and 10° are larger than cases of the model with no stagger in Fig. 9(a). The reason is considered that the angle of the flow behind the model that blows downward is smaller in cases of the staggered model. The flow on the upper surface of the lower element doesn't separate even at 10°.

Figure 10 shows the smoke line visualizations around the biplane configuration with leading and trailing edge flap (δ_n = 15°, δ_f = 30°). The stagger value are 0 and 0.5*c*, respectively. In Fig. 10(a), the smoke lines flow smoothly on the upper surfaces of both upper and lower elements at 0°. At 10°, no flow separation are observed at the leading edge of the upper element. Compare with the results in Fig. 9(a), the effects of the leading-edge flap on reducing the separation on the upper surface of the biplane elements are confirmed. In Fig. 10(b), the vortices near the trailing flap of the upper element are observed. The smoke lines below the model are strongly curved. At 10, the flow near the leading edge of the upper element is separated.

From the results, the leading-edge flap shows the effects on reducing the flow separation on the upper surface of both upper and lower elements. On the other hand, the separation near the leading edge of the upper surface of the upper element is larger in cases of staggered models.

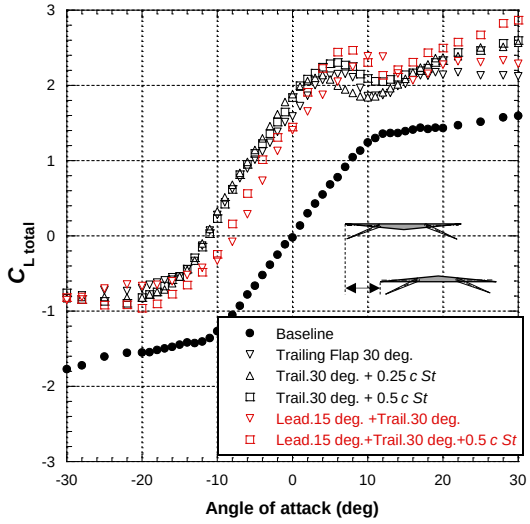

(a) Lift coefficient.

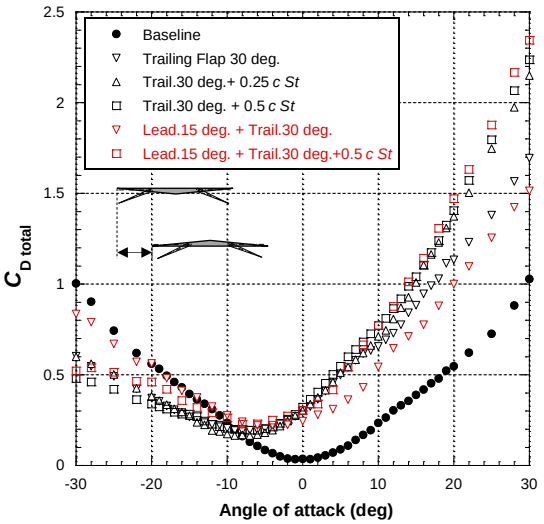

(b) Drag coefficient.

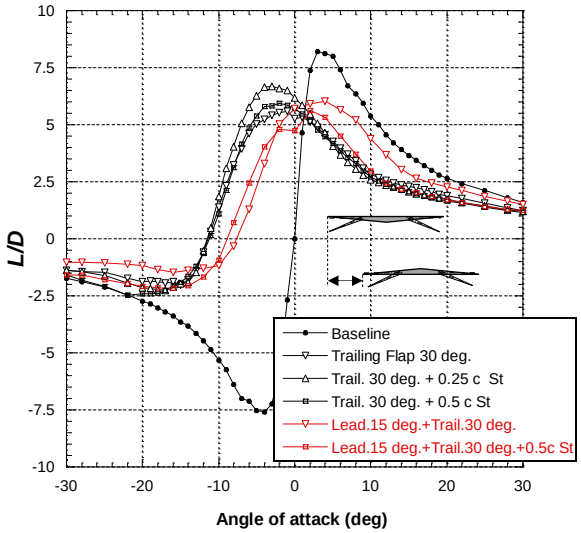

(c) Lift to drag ratio.

Figure 7 The aerodynamic characteristics of Busemann biplane with flaps and stagger.

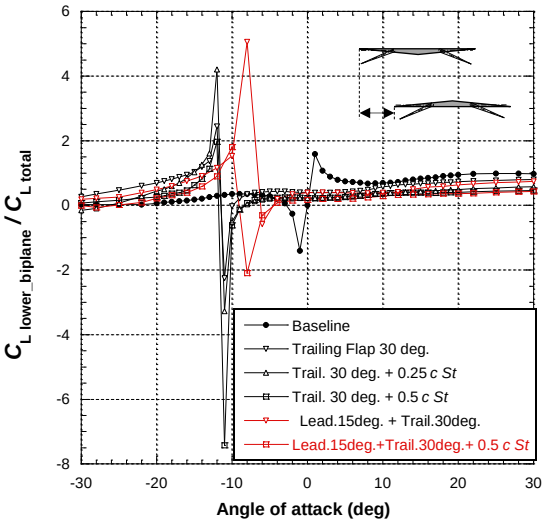

(a) Ratio for lift coefficient.

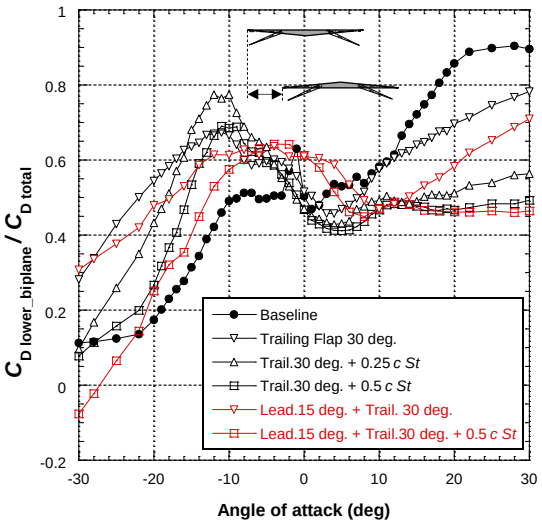

(b) Ratio for drag coefficient.

Figure 8 Ratios of the lower element to the biplane performances with flaps and stagger.

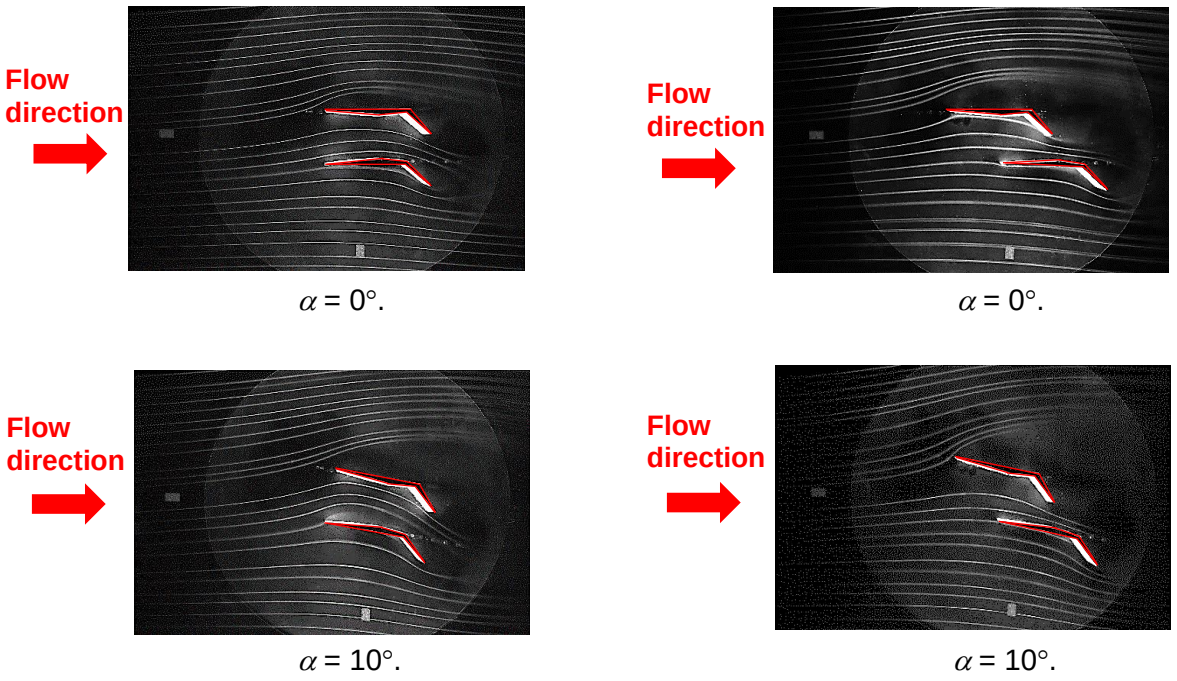

α = 0°. α = 0°.

α = 10°. α = 10°.

(a) No Stagger. (b) 0.5*c* Stagger.

Figure 9 Smoke line visualization of trailing flap and Stagger models. (δ_n = 0°, δ_f = 30°)

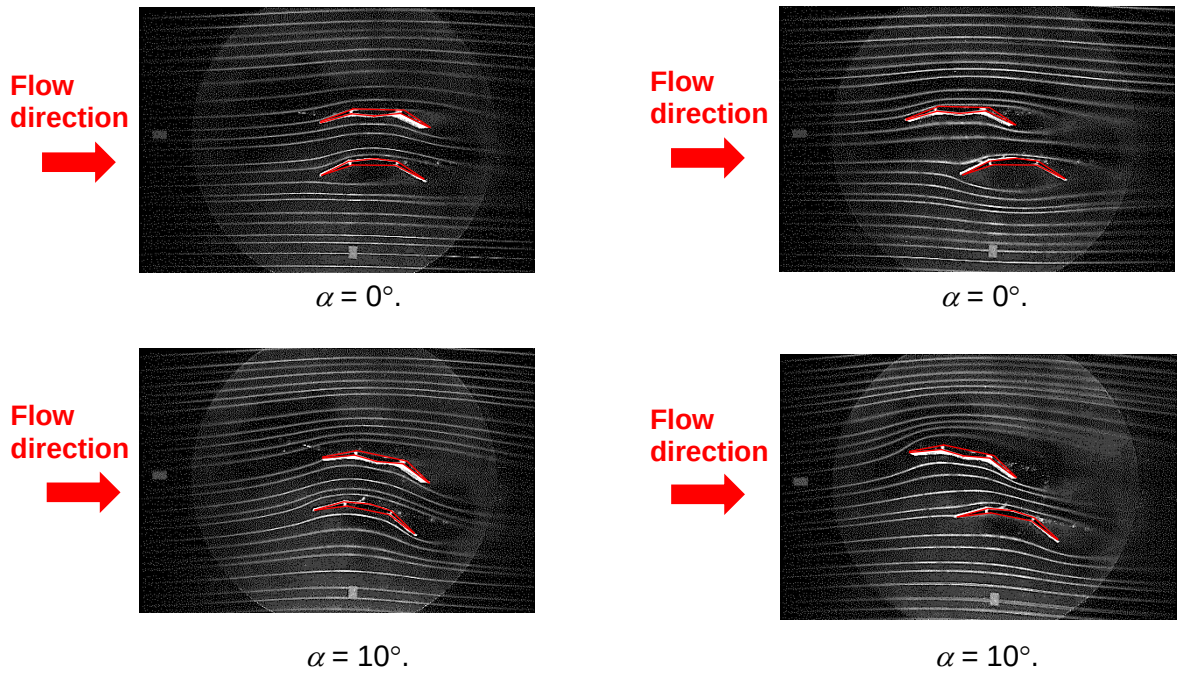

α = 0°. α = 0°.

α = 10°. α = 10°.

(a) No Stagger. (b) 0.5*c* Stagger.

Figure 10 Smoke line visualization of trailing flap and Stagger models. (δ_n = 15°, δ_f = 30°)

Table 3. Lift slopes of biplane configurations (-14° to 4°).

Biplane configuration	**Baseline Ref. [13]**	δ_n **= 0°** δ_f **= 15°**	δ_n **= 0°** δ_f **= 30°**	δ_n **= 0°** δ_f **= 45°**	δ_n **= 15°** δ_f **= 30°**
No Stagger	0.129	0.133	0.14	0.15	0.166
0.25*c* Stagger	0.134	-	0.152	-	-
0.5*c* Stagger	0.144	-	0.155	-	0.173

4. Conclusions

In this paper, the effects of leading-edge and trailing-edge flaps on two-dimensional low-speed performances of the Busemann supersonic biplane are clarified. The stagger models that incorporated flaps were also investigated.

The results of single configurations showed the increment of lift and drag when flaps are installed. The lift slopes are nearly constant when the deflection of the trailing-edge flap increases. The leading-edge flap increases lift slope in both upper and lower elements.

The total lift and drag of the biplane increase when flaps are installed. The lift slope increases when the deflection of the trailing-edge flap increases. The contribution of the lower element to the total lift and drag of the biplane decreases at angles of attack above 0° when flap deflection increases.

The leading-edge flaps and the stagger make the lift slope increase. The flaps and stagger increase the maximum lift, decreasing the stall angle compared with the configuration with only a trailing-edge flap. The stagger also makes the contribution of the lower element to the total lift and drag decrease at angles above 0°. The leading-edge flap reduces the flow separation on the upper surface of both upper and lower elements. In staggered models, the separation near the leading edge of the upper element's upper surface is more extensive than in the biplane model with no stagger.

5. Contact Author Email Address

The contact author email address: thaiduongyh@gmail.com

6. Copyright Statement

References

[1] Kusunose, K, Matsuyama, K, Obayashi, S, Furukawa, T, Kuratani, N, Goto, Y. *Aerodynamic Design of supersonic biplane, cutting edge and related topics.* The 21st century COE Program, International COE of flow dynamic lecture series, Vol. 5, Tohoku Univ. Press, Sendai, Japan, 2007.

[2] Kusunose, K, Matsushima, K, Maruyama, D. Supersonic biplane - A review. *Progress in Aerospace Sciences*, Vol. 47, No. 1, pp 53-87, 2011.

[3] Kuratani, N, Ogawa, T, Yamashita, H, Yonezawa, M and Obayashi, S. Experimental and Computational Fluid Dynamic Around Supersonic Biplane for Sonic Boom Reduction. *AIAA Paper* 2007-3674, 2007.

[4] Nagai, H, Oyama, S, Ogawa, T, Kuratani, N, Asai, K. Experimental Study on Interference Flow of a Supersonic Busemann Biplane using Pressure-Sensitive Paint Technique. *26th International Congress of the Aeronautical Sciences*, 2008.

[5] Yamashita, H, Kuratani, N, Yonezawa, M, Ogawa, T, Nagai, H, Asai, K and Obayashi, S. Wind Tunnel Testing on Start/Unstart Characteristics of Finite Supersonic Biplane Wing. *International Journal of Aerospace Engineering*, 231434, 2013.

[6] Yamashita, H, Yonezawa, M, Obayashi, S, and Kusunose, K. A Study of Busemann-Type Biplane for Avoiding Choked Flow. *AIAA Paper* 2007-0688, 2007.

[7] Yamashita, H, Obayashi, S, Kusunose, K. Reduction of Drag Penalty by means of Plain Flaps in the Boomless Busemann Biplane. *International Journal of Emerging Multidisciplinary Fluid Sciences*, Vol. 1, No. 2, pp 141-164, 2009.

[8] Patidar, V K, Yadav, R, Joshi, S. Numerical investigation of the effect of stagger on the aerodynamic characteristics of a Busemann biplane. *Aerospace Science and Technology*, Vol. 55, pp 252-263, 2016.

[9] Ma, B, Wang, G, Wu, J, and Ye, Z. Avoiding Choked Flow and Flow Hysteresis of Busemann Biplane by Stagger Approach. *Journal of Aircraft*, Vol. 57, No. 3, pp 440-455, 2020.

[10] Kuratani, N, Ozaki, S, Obayashi, S, Ogawa, T, Matsuno, T, and Kawazoe, H. Experimental and Computational Studies of Low-Speed Aerodynamic Performance and Flow Characteristics around a Supersonic Biplane. *Trans. Japan Soc. Aero. Space Sci.*, Vol. 52, pp 89–97, 2009.

[11] Kashitani, M, Yamaguchi, Y, Kai, Y, Hirata, K, and Kusunose, K. Study on Busemann Biplane Airfoil in Low-speed Smoke Wind Tunnel. *Trans. Japan Soc. Aero. Space Sci.*, Vol. 52, pp 213–219, 2010.

[12] Kashitani, M, Nguyen, T D, Taguchi, M, and Kusunose, K. Aerodynamic Characteristics of Busemann Biplane Installed with High-Lift Device Using Low-Speed Smoke Wind Tunnel. *AIAA SciTech Forum*, San Diego, America, AIAA paper 2022-0140, 2022.

[13] Nguyen, T D, Kashitani, M, Taguchi, M and Kusunose, K. Effect of Stagger on Low-speed Performance of Busemann Biplane Airfoil. *Aerospace*, Vol. 9, 197, 2022.

[14] Nguyen, T D, Kashitani, M, Taguchi, M, and Kusunose, K. Evaluation of low-speed aerodynamic characteristics of Busemann biplane airfoil using balance measurement. *59th Aircraft Symposium*, Japan, 3B03, 2021. (In Japanese).

[15] Mueller, T J and Burns T F. Experimental Studies of the Eppler 61 Airfoil at Low Reynold Numbers, *AIAA Paper* 82-0345, 1982.

[16] Nguyen, H A, Mizoguchi, M, Itoh, H. Unsteady Aerodynamic Characteristics of NACA0012 Airfoil Undergoing Constant Pitch-Rate Motions at Low Reynolds Numbers. *Japan Soc. Aero. Space Sci. Aero. Tech.*, Vol. 19, pp 111-119, 2020. (In Japanese).

[17] Jones, R, Cleaver, D J, Gursul, I. Aerodynamics of biplane and tandem wings at low Reynolds numbers. *Experiments in Fluids*, Vol. 56, pp 1-25, 2015.